Transforming Escherichia coli Proteomembranes into Artificial Chloroplasts Using Molecular Photocatalysis

Mengele, Alexander Klaus; Weixler, Dominik; Amthor, Sebastian; Eikmanns, Bernhard J.; Seibold, Gerd M.; Rau, Sven

Published in:
Angewandte Chemie International Edition

Link to article, DOI:
10.1002/anie.202114842

Publication date:
2022

Document Version
Publisher's PDF, also known as Version of record

How to cite: *Angew. Chem. Int. Ed.* **2022,** *61,* e202114842
International Edition: doi.org/10.1002/anie.202114842
German Edition: doi.org/10.1002/ange.202114842

Photocatalysis

Transforming *Escherichia coli* Proteomembranes into Artificial Chloroplasts Using Molecular Photocatalysis

Alexander K. Mengele[+], Dominik Weixler[+], Sebastian Amthor, Bernhard J. Eikmanns, Gerd M. Seibold, and Sven Rau**

Abstract: *During the light-dependent reaction of photosynthesis, green plants couple photoinduced cascades of redox reactions with transmembrane proton translocations to generate reducing equivalents and chemical energy in the form of NADPH (nicotinamide adenine dinucleotide phosphate) and ATP (adenosine triphosphate), respectively. We mimic these basic processes by combining molecular ruthenium polypyridine-based photocatalysts and inverted vesicles derived from Escherichia coli. Upon irradiation with visible light, the interplay of photocatalytic nicotinamide reduction and enzymatic membrane-located respiration leads to the simultaneous formation of two biologically active cofactors, NADH (nicotinamide adenine dinucleotide) and ATP, respectively. This inorganic-biologic hybrid system thus emulates the cofactor delivering function of an active chloroplast.*

Introduction

Although converting just a fraction of the incoming solar energy into chemical bond energy,[1,2] photosynthesis represents a key process enabling the occurrence of sophisticated life on earth.[3] Thus, it also serves as a functional blueprint for the sustainable harvesting and storage of solar energy in the 21st century.[4] With its precisely membrane-organized photosystems (PSs), catalytic subunits and electron transport chains, photon absorption by green plants induces a directed charge separation on the nanoscale provoking the oxidation of water as well as the reductive formation of NADPH (nicotinamide adenine dinucleotide phosphate).[5] Based on the positioning of the catalytic subunits on different sides of the thylakoid membrane and a proton pump integrated in between the two photosystems PSI and PSII, an electrochemical proton gradient (proton motive force, pmf) across the membrane is additionally established. This represents the driving force of ATP (adenosine triphosphate) synthesis via chemiosmotic coupling.[6–8] ATP constitutes the central energy storage molecule within all living systems and is thus a crucial cofactor for many energy-dependent biochemical reactions, such as CO_2 fixation reactions in the Calvin–Benson–Bassham cycle.[9]

Using visible light as a switchable stimulus or energy source, several strategies for the semi-artificial photo-induced production of ATP have been reported.[10] They range from adding non-natural chromophore nanoparticles to intact chloroplasts for improved ATP synthesis[11,12] over bioengineered originally non-photosynthetic microorganisms[13,14] to a variety of bottom-up fabricated liposomes and polymersomes.[15]

As a pmf always represents the ultimate starting point for ATP synthesis, these vesicle systems can be classified by the photo-responsive agent generating the proton gradient. Typically, reconstituted bacteriorhodopsins (bRs),[16–25] photoacids[26–28] or photobases[29] are utilized. Additionally, successful ATP synthesis was triggered by the photoactivity of whole membrane-embedded PSII aggregates releasing protons upon oxidation of water at the Mn_4CaO_5 cluster.[30–32] Moreover, in the presence of hydrophobic quinones acting as proton shuttles, the charge separated excited state of an organic molecular triad was capable of acidifying the inside of a vesicle resulting in the photocatalytic ATP formation at reconstituted ATP synthases.[33,34]

Some of these light-dependent systems made further use of the generated ATP,[23,24,32] e.g. ATP synthesis was coupled to energy demanding cascade reactions such as DNA transcription.[35] It was also shown that the fixation of CO_2 yielding oxaloacetate from pyruvate[32] or even glucose, exploiting all components of the Calvin–Benson–Bassham cycle, can be realized.[22] Furthermore, parallel NADPH and ATP formation by fully functional chloroplasts inside cell-sized droplets were used for a variety of bio-engineered CO_2 fixation processes.[36]

[*] A. K. Mengele,[+] S. Amthor, Prof. S. Rau
Institute of Inorganic Chemistry I
Materials and Catalysis
Ulm University
Albert-Einstein-Allee 11, 89081 Ulm (Germany)
E-mail: sven.rau@uni-ulm.de

D. Weixler,[+] Prof. B. J. Eikmanns, Assoc. Prof. G. M. Seibold
Institute of Microbiology and Biotechnology
Ulm University
Albert-Einstein-Allee 11, 89081 Ulm (Germany)

Assoc. Prof. G. M. Seibold
Section of Synthetic Biology
Department of Biotechnology and Bioengineering
Technical University of Denmark
Søltoftsplads, 2800 Kongens Lyngby (Denmark)

[+] These authors contributed equally to this work.

Beyond this scope, an interlink between the photochemical NADH (reduced nicotinamide adenine dinucleotide) generation with the respiratory electron transport chains[37] would result in a fully functional mimic of a chloroplast's behavior. Therefore, we intended to generate a hybrid system consisting of a molecular photocatalyst providing NADH which is subsequentially consumed by inverted *E. coli* proteomembranes driving the ATP synthesis. These inverted proteomembranes originate directly from *E. coli* cells by a single passage through a French Press.[38–40] Thus, the cell membranes become everted resulting in an inside-out conversion of all membrane proteins present in the *E. coli* cell including the respiratory chain complexes and the ATP-synthase. This inversion brings the valuable advantage of an easy accessibility of the membrane proteins and their reaction products normally present in the intracellular space. Therefore, the generation of a pmf necessary for ATP synthesis can easily be achieved by the addition of NADH to the exterior solution and thereby activating the NADH-dehydrogenase-ubiquinone complex with its proton pumping activity.[41,42] In the presence of ADP and inorganic phosphate (P_i) the *in vitro* ATP-synthesis using these inverted *E. coli* vesicles could be shown, e.g. by an adapted micro-biosensor approach.[43]

Photochemical dyads consisting of a light absorbing moiety coupled to an NADH forming catalytic unit are ideally suited as these heterodinuclear transition metal complexes ensure close spatial proximity between essential components in biologically complex environments. These architectures benefit from ultrafast electron transfers from the chromophoric moiety to the catalytic center via the bridging ligand.[44–47] This efficiently generates a charge separated state which can be quenched in the presence of suitable sacrificial reductants enabling catalytic turnover.

Based on our recent work demonstrating the successful coupling of photochemical NADH formation followed by enzymatic pyruvate reduction[48] we chose the water-soluble dinuclear complex $[(bpy)_2Ru(tpphz)Rh(Cp^*)Cl]Cl_3$ (**1**, bpy = 2,2′-bipyridine, tpphz = tetrapyridophenazine, Cp* = pentamethylcyclopentadienyl) to provide reduced cofactor equivalents to the NADH dehydrogenase of inverted *E. coli* proteomembranes. As the generated ATP is further utilized by hexokinase in an enzymatic phosphorylation reaction, the designed inorganic-biologic hybrid system constitutes a reaction network in which a heterodinuclear photocatalyst finally induces the ATP dependent formation of glucose-6-phosphate (G6P) upon irradiation with visible light (see Scheme 1). Consequently, the presented approach enables a photoinduced simultaneous formation of the two ubiquitous cofactors ATP and NADH which represents a biochemical prerequisite for fully autonomous self-sustaining synthetic protocells.

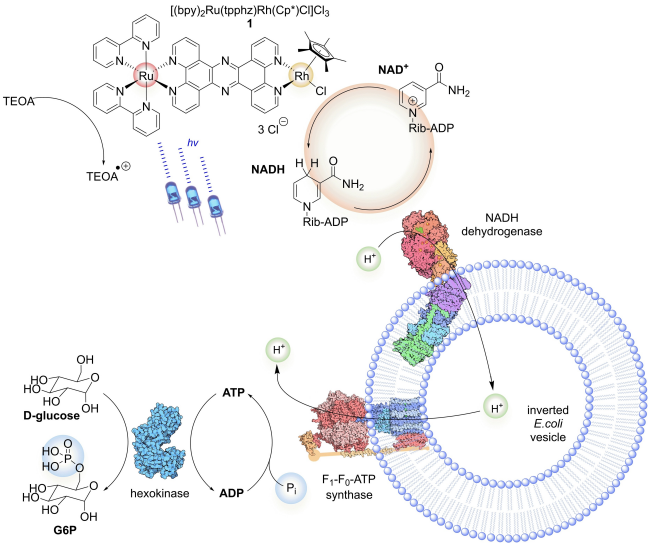

Scheme 1. Schematic overview of the photobiocatalytic process connecting the photocatalytic NADH formation of **1** with the enzymatic ATP and G6P production using inverted *E. coli* vesicles as the central cofactor conversion machinery.

Results and Discussion

The envisaged transition metal complex–inverted *E. coli* vesicle hybrid system was designed to operate with two non-interfering catalytic cycles in an aqueous buffer solution, i.e. the vesicle-independent NADH formation in the exterior bulk solution and the ATP synthesis in the confined space of the proteomembranes using the freely diffusing nicotinamides. In order to minimize possibly detrimental effects of pronounced complex–vesicle interactions, $[(bpy)_2Ru(tpphz)Rh(Cp^*)Cl]Cl_3$ (**1**, see Scheme 1) was chosen as NADH producing photocatalyst, lacking the lipophilicity increasing *tert*-butyl groups on the terminal bpy ligands of the previously investigated heterodinuclear complex used for the photobiocatalytic pyruvate reduction.[48] Following established protocols,[49] **1** was synthesized by stirring $[(bpy)_2Ru(tpphz)]Cl_2$ and $[Rh(Cp^*)Cl_2]_2$ in methanol at room temperature. The resulting complex possesses three chloride counter anions which ensure a high solubility in water (see chapters 5 and 6 of the Supporting Information for detailed synthetic protocols and structural characterization).

Typical for a ruthenium tris-bipyridine like complex, the photocatalyst **1** possesses a broad ^{1}MLCT band in the visible region with $\lambda_{max} = 443$ nm (Figure 1A). Irradiation into this band using one LED-stick ($\lambda_{max} = 465$ nm) for 5 h does not lead to any significant photodecomposition of complex **1** (Figure S1). The photostability of this compound is therefore ensured for the photobiocatalysis experiments since in this case irradiation was typically performed for only 1.5 h. Compared to the mononuclear analog $[(bpy)_2Ru(tpphz)]Cl_2$ (**3**) the ruthenium based emission in **1** is quenched almost completely which indicates efficient intramolecular electron transfer to the Rh center (Figure 1A).[47] This photochemical reductive activation of the catalytic center is a key prerequisite for subsequent regioselective NADH formation.[50]

In fact, the RhCp* center in complex **1** proved to be active in the reduction of NAD^+ (oxidized nicotinamide adenine dinucleotide) to NADH via two chemically orthogonal pathways. First, the light-independent formate-driven

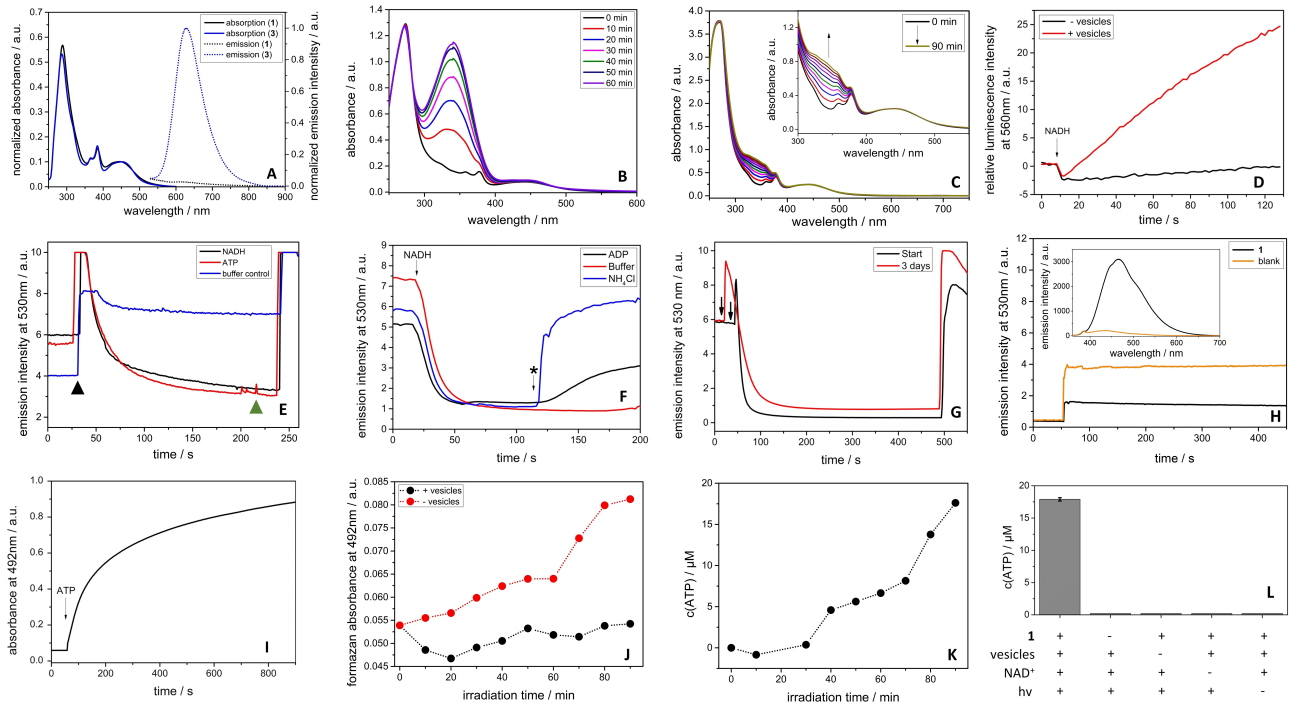

Figure 1. A) Ground-state UV/Vis absorption (solid lines) and steady-state emission spectrum (dotted lines) of the complexes **1** and **3** in DMSO. B) Photo-independent NADH production using **1** (5 µM) and $NaHCO_2$ (100 mM) as chemical reductant. C) Photocatalytic reduction of NAD^+ in the photobiocatalysis buffer, using complex **1** (20 µM). D) Evaluation of the *in vitro* ATP-synthesis with inverted *E. coli* vesicles (650 µg mL^{-1} total protein concentration) using a luminol-luminescence assay. ATP synthesis was monitored at 560 nm in the presence (red curve) or the absence of vesicles (black curve). The black arrow indicates addition of NADH (500 µM final concentration) to initiate the vesicle respiration and the ATP synthesis. E) Emission of AO in the presence of vesicles upon initial addition of the respective substrate (ATP or NADH; 1.0 mM or 0.5 mM final concentration, respectively) or the pure buffer (black triangle) and subsequent addition of NH_4Cl (green triangle). F) Course of the AO fluorescence in the presence of 650 µg mL^{-1} (total protein concentration) of inverted *E. coli* vesicles. As indicated with the first arrow, NADH addition (500 µM, final concentration) initiates respiratory activity of the vesicles. Addition of ADP, NH_4Cl or the pure buffer is indicated with the asterisk marked arrow. G) Course of the AO fluorescence after addition of NADH (500 µM) to 650 µg mL^{-1} (total protein concentration; addition is indicated by the black arrows) of the inverted *E. coli* vesicles which were either used directly (black curve) or irradiated for 3 days at room temperature (red curve) using one LED-stick (λ_{max} = 465 nm, 45–50 mW cm^{-2}). H) Emission of AO in the presence of an independently irradiated photocatalysis mixture with the subsequent addition of the vesicles (t = 50 s). The photocatalysis mixture was irradiated for 2 h in the typical photobiocatalysis buffer (1 mM NAD^+, 25 µM **1** (black trace) or 0 µM **1** (i.e. "blank", orange trace)); the inset shows the emission resulting from the photogenerated NADH ($\lambda_{max} \approx$ 460 nm) after these 2 h of irradiation. I) Course of formazan formation, detected by its absorbance at 492 nm. The mixture consisted of glucose (0.1 mM), hexokinase (1 U), G6P-DH (1 U), $NADP^+$ (0.5 mM), diaphorase (0.8 U) and INT (0.1 mM). The addition of ATP (0.5 mM, final concentration) is indicated by the black arrow and induces the enzymatic reaction cascade depicted in Scheme S1. J) Exemplary kinetic analysis of the photogenerated NADH by formazan absorbance at 492 nm after workup of the aliquots taken from the photobiocatalysis at the given irradiation time using 5 µM **1** as catalyst (see also Figures S5 and S10). K) Exemplary kinetic development of ATP concentration during the photobiocatalysis using 5 µM **1** as the catalyst (see also Figure S5). L) Comparison of the ATP output from different catalysis mixtures using 5 µM of catalyst **1**.

nicotinamide reduction verified the catalytic ability of the RhCp* moiety as indicated by formation of the characteristic 340 nm band of NADH (Figure 1B).[50] Next, also the photoinduced NADH formation occurred under conditions later used for combining the photocatalyst and the inverted vesicles (Figure 1C; 50 mM BTP (bis-tris propane), 140 mM choline chloride, 5 mM $MgCl_2$, 5 mM Na_3PO_4, 1 mM NAD^+ and 0.2 M triethanolamine (TEOA) at pH 8.0). Here, TEOA served as sacrificial reducing agent regenerating the Ru^{II} state of the photooxidized Ru^{III} center, hence preventing deleterious recombination of the metal based charge separated state.[47] Consequently, no NADH formation was observed in the absence of TEOA (Figure S2). **1** is therefore capable to photocatalytically generate NADH under biologically compatible reaction conditions.

The inverted *E. coli* vesicles were generated as previously described elsewhere.[43] Depending on different batches, the inverted vesicles had a total protein content of 20–30 µg µL^{-1}. To assess the ability of the prepared inverted vesicles to synthesize ATP *in vitro*, a qualitative luminiol/luciferase assay was used (Figure 1D). Here, the successful ATP formation after addition of NADH was monitored by increasing luminescence values. Previously it could be shown that ATP synthesis is indeed driven by the ATP synthase present in the membrane of the vesicles since addition of 2 µM of the ATP synthase inhibitor venturicidin A completely suppressed the ATP synthesis capacity of the *E. coli* inverted membrane vesicles.[43]

To evaluate an appropriate amount of vesicles and NADH for the *in vitro* ATP-synthesis a quantitative

luminiol/luciferase assay was used (Figure S3). Based on these data, the NADH concentration was set to 500 μM and the amount of vesicles was adjusted to 0.65 μg μL^{-1} total protein content for every further experiment.

Next, the vesicles' ability to generate a pmf by oxidation of NADH was examined in detail using an acridine orange assay (AO assay). The fluorophore AO is able to accumulate inside the vesicles by following the proton gradient across the membrane leading to the quenching of AO fluorescence due to the reduced absorbance of the formed dimeric AO aggregate at the chosen excitation wavelength.[51] As expected, addition of NADH to the buffered vesicle solution led to the formation of a proton gradient across the vesicle membrane indicated by a decreasing AO fluorescence (Figure 1E). As depicted in Figure 1E as well, also the addition of ATP to the reaction mixture resulted in an acidification of the vesicle demonstrating the known ATPase activity of the F_1F_O-ATP synthase present in the membrane.[52–54] The respective buffer control resulted in no AO quenching compared to the addition of NADH and ATP. As the NADH-induced formation of a proton gradient was also abolished upon the subsequent addition of ADP (Figure 1F), the inverted *E. coli* vesicles work as depicted in Scheme 1. The order of biochemical events can thus be described by an NADH oxidation-induced vesicle acidification followed by the conversion of ADP into ATP.

The capacity of proton gradient formation after the addition of NADH was also evaluated after several days of irradiation of a vesicle solution using a blue light emitting LED-stick (λ_{max} = 465 nm). As revealed by the AO assay, formation of a typical proton gradient across the *E. coli* vesicle membrane could be observed even after 3 days of constant irradiation indicating the excellent photostability of the vesicles needed for further photobiocatalytic experiments (Figure 1G).

After confirming the photostability as well as the catalytic activity of the separate systems, i.e. photocatalytic NADH-formation by **1** and productive NADH consumption by the inverted *E. coli* vesicles, combination of these independent catalytic entities to achieve the final synergistic hybrid system was performed. In a first step, however, the individual processes were still separated spatially and temporarily in order to evaluate whether NADH generated by **1** in the absence of the inverted *E. coli* vesicles in fact initiated the formation of a proton gradient when brought in contact with the proteomembranes. After irradiating 1 mM NAD^+ in the presence or the absence of 25 μM **1** for 2 h in the typical buffer used for photobiocatalysis experiments (see above), emission spectroscopy verified the formation of reduced nicotinamides only when **1** was present (Figure 1H). Subsequently, AO was added to these solutions and emission at 530 nm was recorded. After an equilibration period, vesicles were injected into the solutions and in contrast to the sample without photocatalyst **1** being present in solution, the observed emission increase was much less pronounced for the sample which did contain **1** during a 2 h lasting irradiation process prior to vesicle addition. As a result of the above-described AO accumulation inside the vesicles, which is associated with lowered emission intensity at 530 nm, this indicates the formation of a proton gradient by the successful consumption of photocatalytically generated NADH (see also Figure S4).

Next, the simultaneous formation of NADH and ATP by the full photobiocatalytic hybrid system was intended. However, since NADH formation using **1** did only proceed gradually (Figure 1C), reverse proton pumping of the vesicles at the expense of ATP hydrolysis (Figure 1E) had to be prohibited. This was achieved using hexokinase-catalyzed G6P formation, trapping the reactive phosphate moiety of ATP on the glucose backbone (see Scheme S1). The equilibrium of the hexokinase reaction is clearly located at the product side.[55] Although it was reported that the product G6P can diminish the activity of hexokinase up to 54 %,[56] the utilization of an excess of hexokinase and long reaction times should make inhibition of the hexokinase activity neglectable. Therefore, a quantitative phosphate transfer from ATP to glucose forming G6P in a quantitative manner can be assumed. Based on a 1:1 stoichiometry, this allows calculation of present ATP levels by enzymatic G6P quantification.

In order to quantify photocatalytically generated G6P, oxidation to the corresponding 6-phospho-δ-lactone using glucose-6-phosphate dehydrogenase (G6P-DH) and $NADP^+$ as cofactor was performed. This step occurred during the workup of the aliquots taken from the photobiocatalysis. Due to the overlapping absorbance with the Ru complexes, the hereby generated NADPH was not analyzed directly. On the contrary, the NADPH dependent diaphorase-catalyzed reductive ring-opening of the tetrazole derivative INT (3-(4-Iodophenyl)-2-(4-nitrophenyl)-5-phenyl-2*H*-tetrazol-3-ium chloride), yielding the pinkish formazan form (λ_{max} = 492 nm), was coupled to the aforementioned reaction (Figure 1I and Scheme S1). This method additionally allowed the verification of the biochemical usability of the photogenerated NADH by a second enzymatic method: Analysis of a photobiocatalytic control experiment excluding the vesicles resulted in the formation of formazan (Figure 1J; the diaphorase also utilizes NADH as cofactor for the reductive ring-opening reaction). In contrast, the presence of the vesicles was inhibiting the NADH-dependent formation of formazan thus showing that the photocatalytically generated NADH was in fact consumed via the respiratory activity of the added *E. coli* vesicles.

Based on these promising results, the full photobiocatalytic system as depicted in Scheme 1 was then examined. In accordance with the obtained results showing only a small dependence of the synthesized ATP with varying NADH concentrations (Figure S3), two different concentrations of **1** (5 and 25 μM) both resulted in the photobiocatalytic formation of similar amounts of G6P, i.e. 15.0 ± 1 μM ATP (corresponding to the amount of formed G6P) using 25 μM of **1** and 17.9 ± 0.3 μM ATP utilizing 5 μM of **1** (Figure 1L). Hence, using 5 μM **1**, the process of photo-induced ATP (G6P) formation can be described as catalytic with respect to **1** (TON ≈ 3.6 ± 0.1). As outlined in chapter 2 of the Supporting Information, a rough calculation on the energy efficiency of this process with 5 μM **1** considering the

amount of absorbed photons yields a value of ca. 3×10^{-3} %. For a system exclusively focusing on ATP formation, an energy efficiency of up to 4 % was reported.[34] Moreover, as shown in Figure 1K, the ATP (G6P) levels were constantly increasing during irradiation (see also Figure S5).

To verify the necessity of all incorporated components contributing to the overall process, exclusion experiments were performed omitting either photocatalyst **1**, the vesicles, NAD^+ or keeping the solution for 90 min in the dark. In none of these cases was ATP (G6P) detected (Figure 1L). Consequently, the reaction sequence shown in Scheme 1 correctly describes the molecular processes that occur. The system consists of a visible light-dependent photoredox catalytic process yielding NADH, followed by the respiratory consumption of the nicotinamides at the vesicle-integrated NADH dehydrogenase. The generated proton gradient ultimately provokes ATP production leading to the subsequent G6P synthesis by G6P-DH.

E. coli, from which the proteomembrane vesicles originate, is a facultatively anaerobic bacterium and possess two types of NADH dehydrogenases (Ndh, NuoA-N) differing in their activity depending on the presence or the absence of oxygen.[57–59] However, both are expressed under the applied aerobic growth conditions.[60] Thus, it enables the bacterium to generate a pmf and consequently also ATP even in the absence of oxygen, conditions that are necessary for the photocatalytic NADH formation utilizing photocatalyst **1**.[61] For comparison, using membrane vesicles originating from the strictly aerobic *Pseudomonas putida* resulted in no photocatalytic ATP formation using **1** as catalyst (data not shown). This is rationalized by the observation that also no ATP was formed when NADH was simply added to these vesicles under exclusion of oxygen. Unlike that, in the presence of oxygen these vesicles did show the capacity for ATP production upon NADH addition.[43]

To further investigate the interplay of Ru complexes and the inverted *E. coli* vesicles, additional experiments were performed. The use of $[Ru(bpy)_3]Cl_2$ (**4**) as photoredox active reference complex resulted in no detectable ATP formation. Since **4** exhibits appropriate photostability (Figure S1), the inactivity can be correlated to the inability of photocatalytic NADH production as it lacks the RhCp* catalyst moiety (Figures S6–S8). Contrary, using $[(bpy)_2Ru(tpphz)]Cl_2$ (**3**), a concentration dependent ATP formation was observed (Figure S9). In addition to the small amounts of NADH that were generated upon irradiation as reported previously (Figures S4, S7),[48] we mainly associate this finding with the interaction of this complex with the proteomembranes via its tpphz ligand. This is verified by an increasing emission of **3** upon vesicle addition (Figure 2A).[62,63]

According to recent literature, such interactions possibly enable other pathways of ATP formation.[64,65] To test this, we utilized $[(bpy^P)_2Ru(tpphz)]Br_2$ (**5**) (bpy^P = (2,2′-bipyridine-4,4′- diylbis(methylene))bis(phosphonic acid)) which is —like the lipids present in the inner *E. coli* membranes[66,67] —negatively charged under the slightly basic buffer conditions.[68] With this anionic complex, significantly reduced interactions with the inverted *E. coli* membranes were detected (Figure 2B, C and S11) and consequently no ATP formation was observed. As for the heterodinuclear analog $[(bpy^P)_2Ru(tpphz)Rh(Cp^*)Br]Br_3$ (**2**) similar ATP (G6P) amounts (22.8 ± 0.8 µM, using 5 µM **2**; TON ≈ 4.6 ± 0.2, see also Figure S12) as for complex **1** were obtained, the modified bpy ligands do neither impart photoredox activity (Figure S7) nor NADH consumption by the *E. coli* vesicles

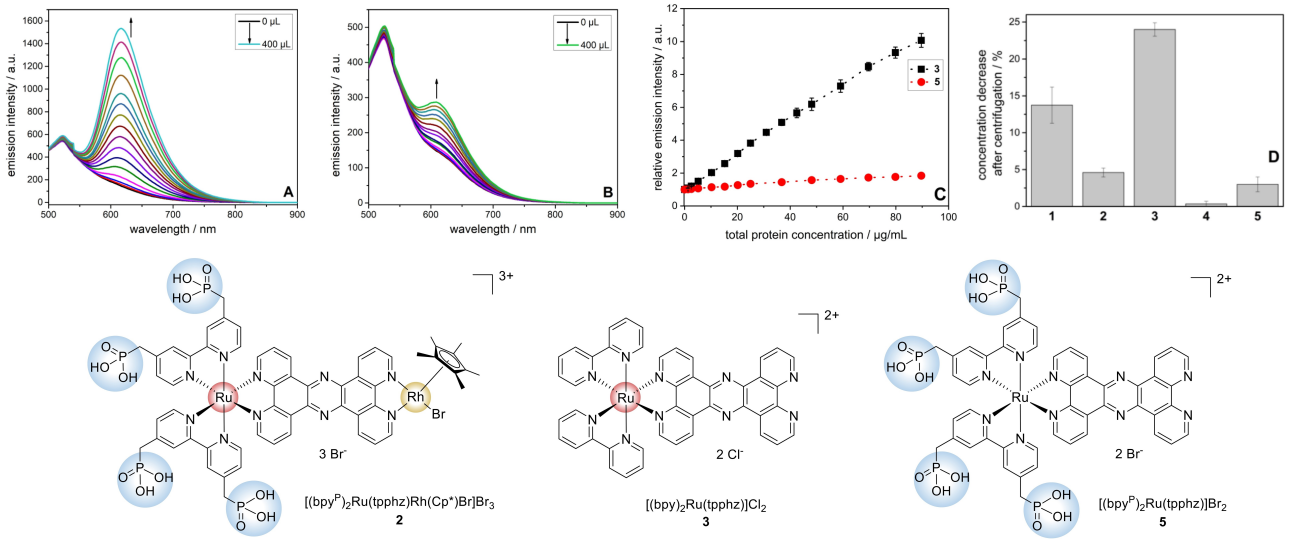

Figure 2. A) and B) Changes of the luminescence intensity of complexes **3** (A) and **5** (B) (both 10 µM and dissolved in the photobiocatalysis buffer) upon addition of increasing volumes of the vesicle suspension (650 µg mL^{-1}). C) Comparison of the relative emission intensity increase of complexes **3** and **5** upon addition of the vesicles (650 µg mL^{-1}, N = 2; the errors are small and are thus mostly overlayed by the data points). D) Evaluation of complex-vesicle interactions by comparing the ground-state UV/Vis absorption spectra of the respective complexes prior and after an 1 h long incubation at room temperature (see Figure S13 for detailed spectra, N = 2). Bottom: Molecular structures of the complexes **2**, **3** and **5**. The phosphonic acid groups highlighted by blue color become deprotonated under the utilized buffer conditions.[68]

(Figure S12). Instead, the inability of **5** to effectively interact with the membranes impedes ATP formation.

These interaction studies via emission spectroscopy were complemented by incubation-centrifugation experiments analyzed by UV/Vis absorption spectroscopy (Figure 2D and Figure S13 for detailed spectra). The loss of ruthenium complex in the supernatant solution by loading the vesicles with the chromophores was much stronger for **3** than for **5**. This trend was also observed for the heterodinuclear complexes as **1** was sticking to the vesicles at a higher extent than **2**. As complex **4** did not stain the vesicles at all, lipophilicity as well as overall charge both contribute to the interaction of Ru complexes and the inverted *E. coli* vesicles. Thus, in the case of lipophilic complexes, the interaction with the vesicles can be decreased by incorporation of anionic functional groups.

To delineate a full picture of the photocatalytic ATP formation in the present system, the detection of a proton gradient in the absence of NAD^+ and ADP was intended. After optimizing the reaction conditions (see Figures S14–S17), 20 μM ruthenium complex (**1**, **3** or **5**) and 5 μM AO were used for monitoring the visible light-driven acidification of the vesicles. Consistent with catalytic outcomes, light-switch results and the centrifugation experiments (Figure 2), a proton gradient in the absence of NAD^+ was only detected for complex **3** (Figures S18, S19).[64,65]

Based on the obtained data, it can thus be concluded that the heterodinuclear complexes **1** and **2** induce the visible light-driven ATP synthesis exclusively via an NAD^+ dependent pathway as schematically depicted in Scheme 1. In view of their ability to imitate a chloroplast's behavior by simultaneously generating NADH as well as ATP, the heterodinuclear Ru–Rh complexes **1** and **2** in combination with inverted *E. coli* vesicles are emphasized for their use in future self-sustaining synthetic protocells.

Conclusion

The presented hybrid system consisting of the heterodinuclear tpphz-bridged Ru–Rh photocatalysts and inverted *E. coli* vesicles is capable of generating the two biologically active cofactors NADH and ATP simultaneously using visible light as external energy source. It therefore imitates the main function of natural chloroplasts to provide reduced nicotinamides as well as ATP for subsequent energy-requiring reductive cascade reactions. By analyzing the individual processes necessary to synthesize ATP, it was shown that the photocatalytically generated NADH in fact acidifies the inside of the proteomembrane vesicles. This resulting pmf is then used to convert ADP and P_i into ATP, finally resulting in the phosphorylation of glucose. This last step is reminiscent of the natural chloroplast system as well, since in green plants photochemically generated ATP is utilized in a biochemically similar phosphorylation reaction to activate ribulose-5-phosphate for CO_2 fixation and reduction.

Additionally, it was found that the interactions of the investigated Ru polypyridine complexes and *E. coli* derived vesicles can be controlled by the overall charge and lipophilicity of the coordination compounds. We find that in accordance with the presence of negatively charged lipids in the vesicle membrane, the negatively charged methylphosphonate derivatives **2** and **5** show significantly lower affinity to the vesicles. The combination between **2** and the proteomembrane vesicles therefore represent a system in which the photocatalytic NADH formation and the subsequent pmf triggered ATP generation are decoupled with minimal electrostatic interactions.

With these results at hand further applications such as cascade reactions utilizing both cofactors NADH and ATP can be envisaged. Energy-intensive reductive activations of N_2 as well as CO_2 fixation reactions might be possible if suitable enzymes would be provided to the presented cofactor-producing inorganic–biologic hybrid system. For such cascade reactions, the system is benefiting from the fact that the generated cofactors are well accessible in the exterior bulk solution rendering it unnecessary to imbed the required enzymes in the vesicular architectures. Hence, our system paves the way towards self-sustaining synthetic protocells which are able to produce reducing equivalents and molecular energy equivalents autonomously, provided they receive suitable photonic input.

Acknowledgements

Supported by the Deutsche Forschungsgemeinschaft (DFG, German Research Foundation)–Projektnummern 364549901–TRR 234 [A1,B2]. Work of GMS was partially funded by the Novo Nordisk Fonden within the framework of the Fermentation-based Biomanufacturing Initiative (FBM) (FBM-grant: NNF17SA0031362). Protein figures integrated into Scheme 1 and the table of contents graphic were obtained from RCSB PDB (Molecule of the Month illustrations, David S. Goodsell; hexokinase: doi:10.2210/rcsb_pdb/mom_2004_2; ATP synthase: doi:10.2210/rcsb_pdb/mom_2005_12; NADH dehydrogenase: doi:10.2210/rcsb_pdb/mom_2011_12) and are utilized under a CC-BY-4.0 license. Open Access funding enabled and organized by Projekt DEAL.

Conflict of Interest

The authors declare no conflict of interest.

Data Availability Statement

The data that support the findings of this study are available from the corresponding author upon reasonable request.

Keywords: Biocatalysis · Cofactors · Photocatalysis · Photosynthesis · Synthetic Biology

[1] R. E. Blankenship, D. M. Tiede, J. Barber, G. W. Brudvig, G. Fleming, M. Ghirardi, M. R. Gunner, W. Junge, D. M. Kramer, A. Melis, et al., *Science* **2011**, *332*, 805–809.
[2] H. Michel, *Angew. Chem. Int. Ed.* **2012**, *51*, 2516–2518; *Angew. Chem.* **2012**, *124*, 2566–2568.
[3] W. W. Fischer, J. Hemp, J. E. Johnson, *Annu. Rev. Earth Planet. Sci.* **2016**, *44*, 647–683.
[4] D. G. Nocera, *Acc. Chem. Res.* **2012**, *45*, 767–776.
[5] Y. Tachibana, L. Vayssieres, J. R. Durrant, *Nat. Photonics* **2012**, *6*, 511–518.
[6] D. M. Kramer, J. A. Cruz, A. Kanazawa, *Trends Plant Sci.* **2003**, *8*, 27–32.
[7] T. Uchihashi, R. Iino, T. Ando, H. Noji, *Science* **2011**, *333*, 755–758.
[8] A. Hahn, J. Vonck, D. J. Mills, T. Meier, W. Kühlbrandt, *Science* **2018**, *360*, eaat4318.
[9] K. Biel, I. Fomina, *Photosynthetica* **2015**, *53*, 161–167.
[10] S. Fukuzumi, Y.-M. Lee, W. Nam, *ChemPhotoChem* **2018**, *2*, 121–135.
[11] Y. Wang, S. Li, L. Liu, F. Lv, S. Wang, *Angew. Chem. Int. Ed.* **2017**, *56*, 5308–5311; *Angew. Chem.* **2017**, *129*, 5392–5395.
[12] Y. Xu, J. Fei, G. Li, T. Yuan, X. Xu, C. Wang, J. Li, *Angew. Chem. Int. Ed.* **2018**, *57*, 6532–6535; *Angew. Chem.* **2018**, *130*, 6642–6645.
[13] A. Martinez, A. S. Bradley, J. R. Waldbauer, R. E. Summons, E. F. DeLong, *Proc. Natl. Acad. Sci. USA* **2007**, *104*, 5590–5595.
[14] E. T. Johnson, C. Schmidt-Dannert, *Trends Biotechnol.* **2008**, *26*, 682–689.
[15] G. Wang, K. Castiglione, *Catalysts* **2019**, *9*, 12.
[16] E. Racker, W. Stoeckenius, *J. Biol. Chem.* **1974**, *249*, 662–663.
[17] N. Wagner, M. Gutweiler, R. Pabst, K. Dose, *Eur. J. Biochem.* **1987**, *165*, 177–183.
[18] B. Pitard, P. Richard, M. Dunach, G. Girault, J.-L. Rigaud, *Eur. J. Biochem.* **1996**, *235*, 769–778.
[19] A. Hazard, C. Montemagno, *Arch. Biochem. Biophys.* **2002**, *407*, 117–124.
[20] H.-J. Choi, C. D. Montemagno, *Nano Lett.* **2005**, *5*, 2538–2542.
[21] T.-J. M. Luo, R. Soong, E. Lan, B. Dunn, C. Montemagno, *Nat. Mater.* **2005**, *4*, 220–224.
[22] D. Wendell, J. Todd, C. Montemagno, *Nano Lett.* **2010**, *10*, 3231–3236.
[23] S. Dhir, S. Salahub, A. S. Mathews, S. K. Kumaran, C. D. Montemagno, S. Abraham, *Chem. Commun.* **2018**, *54*, 5346–5349.
[24] S. Berhanu, T. Ueda, Y. Kuruma, *Nat. Commun.* **2019**, *10*, 1325.
[25] C. Kleineberg, C. Wölfer, A. Abbasnia, D. Pischel, C. Bednarz, I. Ivanov, T. Heitkamp, M. Börsch, K. Sundmacher, T. Vidaković-Koch, *ChemBioChem* **2020**, *21*, 2149–2160.
[26] Y. Xu, J. Fei, G. Li, T. Yuan, J. Li, *ACS Nano* **2017**, *11*, 10175–10183.
[27] Y. Xu, J. Fei, G. Li, T. Yuan, Y. Li, C. Wang, X. Li, J. Li, *Angew. Chem. Int. Ed.* **2017**, *56*, 12903–12907; *Angew. Chem.* **2017**, *129*, 13083–13087.
[28] Y. Li, X. Feng, A. Wang, Y. Yang, J. Fei, B. Sun, Y. Jia, J. Li, *Angew. Chem. Int. Ed.* **2019**, *58*, 796–800; *Angew. Chem.* **2019**, *131*, 806–810.
[29] G. Li, J. Fei, Y. Xu, J.-D. Hong, J. Li, *J. Colloid Interface Sci.* **2019**, *535*, 325–330.
[30] X. Feng, Y. Jia, P. Cai, J. Fei, J. Li, *ACS Nano* **2016**, *10*, 556–561.
[31] Y. Li, J. Fei, G. Li, H. Xie, Y. Yang, J. Li, Y. Xu, B. Sun, J. Xia, X. Fu, et al., *ACS Nano* **2018**, *12*, 1455–1461.
[32] K. Y. Lee, S.-J. Park, K. A. Lee, S.-H. Kim, H. Kim, Y. Meroz, L. Mahadevan, K.-H. Jung, T. K. Ahn, K. K. Parker, et al., *Nat. Biotechnol.* **2018**, *36*, 530–535.
[33] G. Steinberg-Yfrach, P. A. Liddell, S.-C. Hung, A. L. Moore, D. Gust, T. A. Moore, *Nature* **1997**, *385*, 239–241.
[34] G. Steinberg-Yfrach, J.-L. Rigaud, E. N. Durantini, A. L. Moore, D. Gust, T. A. Moore, *Nature* **1998**, *392*, 479–482.
[35] E. Altamura, P. Albanese, R. Marotta, F. Milano, M. Fiore, M. Trotta, P. Stano, F. Mavelli, *Proc. Natl. Acad. Sci. USA* **2021**, *118*, e2012170118.
[36] T. E. Miller, T. Beneyton, T. Schwander, C. Diehl, M. Girault, R. Mclean, T. Chotel, P. Claus, N. S. Cortina, J. Baret, et al., *Science* **2020**, *368*, 649–654.
[37] M. Saraste, *Science* **1999**, *283*, 1488–1493.
[38] S. V. Ambudkar, G. W. Zlotnick, B. P. Rosen, *J. Biol. Chem.* **1984**, *259*, 6142–6146.
[39] H. Sze, *Ann. Rev. Plant Physiol.* **1985**, *36*, 175–208.
[40] E. B. Goldberg, T. Arbel, J. Chen, R. Karpel, G. A. Mackie, S. Schuldiner, E. Padan, *Proc. Natl. Acad. Sci. USA* **1987**, *84*, 2615–2619.
[41] K. Matsushita, T. Ohnishi, H. R. Kaback, *Biochemistry* **1987**, *26*, 7732–7737.
[42] A. Wiedenmann, P. Dimroth, C. von Ballmoos, *Mol. Microbiol.* **2009**, *72*, 479–490.
[43] J. Lin, D. Weixler, S. Daboss, G. M. Seibold, C. Andronescu, W. Schuhmann, C. Kranz, *Talanta* **2019**, *205*, 120083.
[44] S. Tschierlei, M. Presselt, C. Kuhnt, A. Yartsev, T. Pascher, V. Sundström, M. Karnahl, M. Schwalbe, B. Schäfer, S. Rau, et al., *Chem. Eur. J.* **2009**, *15*, 7678–7688.
[45] M. G. Pfeffer, T. Kowacs, M. Wächtler, J. Guthmuller, B. Dietzek, J. G. Vos, S. Rau, *Angew. Chem. Int. Ed.* **2015**, *54*, 6627–6631; *Angew. Chem.* **2015**, *127*, 6727–6731.
[46] M. G. Pfeffer, B. Schäfer, G. Smolentsev, J. Uhlig, E. Nazarenko, J. Guthmuller, C. Kuhnt, M. Wächtler, B. Dietzek, V. Sundström, et al., *Angew. Chem. Int. Ed.* **2015**, *54*, 5044–5048; *Angew. Chem.* **2015**, *127*, 5132–5136.
[47] L. Zedler, A. K. Mengele, K. M. Ziems, Y. Zhang, M. Wächtler, S. Gräfe, T. Pascher, S. Rau, S. Kupfer, B. Dietzek, *Angew. Chem. Int. Ed.* **2019**, *58*, 13140–13148; *Angew. Chem.* **2019**, *131*, 13274–13282.
[48] A. K. Mengele, G. M. Seibold, B. J. Eikmanns, S. Rau, *ChemCatChem* **2017**, *9*, 4369–4376.
[49] U. Kölle, M. Grätzel, *Angew. Chem. Int. Ed. Engl.* **1987**, *26*, 567–570; *Angew. Chem.* **1987**, *99*, 572–574.
[50] H. C. Lo, C. Leiva, O. Buriez, J. B. Kerr, M. M. Olmstead, R. H. Fish, *Inorg. Chem.* **2001**, *40*, 6705–6716.
[51] M. G. Palmgren, *Anal. Biochem.* **1991**, *192*, 316–321.
[52] G. Vogel, R. Steinhart, *Biochemistry* **1976**, *15*, 208–216.
[53] N. B. Shah, M. L. Hutcheon, B. K. Haarer, T. M. Duncan, *J. Biol. Chem.* **2013**, *288*, 9383–9395.
[54] O. Biner, J. G. Fedor, Z. Yin, J. Hirst, *ACS Synth. Biol.* **2020**, *9*, 1450–1459.
[55] F. Meurer, M. Bobrownik, G. Sadowski, C. Held, *Biochemistry* **2016**, *55*, 5665–5674.
[56] H. Gao, J. A. Leary, *J. Am. Soc. Mass Spectrom.* **2003**, *14*, 173–181.
[57] G. Unden, J. Bongaerts, *Biochim. Biophys. Acta Bioenerg.* **1997**, *1320*, 217–234.
[58] T. Friedrich, *Biochim. Biophys. Acta Bioenerg.* **1998**, *1364*, 134–146.
[59] G. Unden, P. A. Steinmetz, P. Degreif-Dünnwald, *EcoSalPlus* **2014**, https://doi.org/10.1128/ecosalplus.ESP-0005-2013.
[60] M. W. Calhoun, K. L. Oden, R. B. Gennis, M. J. T. de Mattos, O. M. Neijssel, *J. Bacteriol.* **1993**, *175*, 3020–3025.
[61] A. K. Mengele, D. Weixler, A. Chettri, M. Maurer, F. L. Huber, G. M. Seibold, B. Dietzek, B. J. Eikmanns, S. Rau, *Chem. Eur. J.* **2021**, *27*, 16840–16845.

[62] M. Ardhammar, P. Lincoln, B. Nordén, *J. Phys. Chem. B* **2001**, *105*, 11363–11368.
[63] F. R. Svensson, M. Li, B. Nordén, P. Lincoln, *J. Phys. Chem. B* **2008**, *112*, 10969–10975.
[64] D. Hvasanov, J. R. Peterson, P. Thordarson, *Chem. Sci.* **2013**, *4*, 3833–3838.
[65] P. Gai, W. Yu, H. Zhao, R. Qi, F. Li, L. Liu, F. Lv, S. Wang, *Angew. Chem. Int. Ed.* **2020**, *59*, 7224–7229; *Angew. Chem.* **2020**, *132*, 7291–7296.
[66] P. M. Oliver, J. A. Crooks, M. Leidl, E. J. Yoon, A. Saghatelian, D. B. Weibel, *J. Bacteriol.* **2014**, *196*, 3386–3398.
[67] V. W. Rowlett, V. K. P. S. Mallampalli, A. Karlstaedt, W. Dowhan, H. Taegtmeyer, W. Margolin, H. Vitrac, *J. Bacteriol.* **2017**, *199*, e00849-16.
[68] M. Montalti, S. Wadhwa, W. Y. Kim, R. A. Kipp, R. H. Schmehl, *Inorg. Chem.* **2000**, *39*, 76–84.

Manuscript received: November 2, 2021
Accepted manuscript online: December 21, 2021
Version of record online: January 28, 2022